Transitional–turbulent spots and turbulent–turbulent spots in boundary layers

Xiaohua Wu[a], Parviz Moin[b,1], James M. Wallace[c], Jinhie Skarda[b], Adrián Lozano-Durán[b], and Jean-Pierre Hickey[a]

[a]Department of Mechanical and Aerospace Engineering, Royal Military College of Canada, Kingston, ON, Canada K7K 7B4; [b]Center for Turbulence Research, Stanford University, Stanford, CA 94305-3035; and [c]Department of Mechanical Engineering, University of Maryland, College Park, MD 20742

Contributed by Parviz Moin, May 4, 2017 (sent for review March 23, 2017; reviewed by John Kim, Beverley McKeon, and Ömer Savaş)

Two observations drawn from a thoroughly validated direct numerical simulation of the canonical spatially developing, zero-pressure gradient, smooth, flat-plate boundary layer are presented here. The first is that, for bypass transition in the narrow sense defined herein, we found that the transitional–turbulent spot inception mechanism is analogous to the secondary instability of boundary-layer natural transition, namely a spanwise vortex filament becomes a Λ vortex and then, a hairpin packet. Long streak meandering does occur but usually when a streak is infected by a nearby existing transitional–turbulent spot. Streak waviness and breakdown are, therefore, not the mechanisms for the inception of transitional–turbulent spots found here. Rather, they only facilitate the growth and spreading of existing transitional–turbulent spots. The second observation is the discovery, in the inner layer of the developed turbulent boundary layer, of what we call turbulent–turbulent spots. These turbulent–turbulent spots are dense concentrations of small-scale vortices with high swirling strength originating from hairpin packets. Although structurally quite similar to the transitional–turbulent spots, these turbulent–turbulent spots are generated locally in the fully turbulent environment, and they are persistent with a systematic variation of detection threshold level. They exert indentation, segmentation, and termination on the viscous sublayer streaks, and they coincide with local concentrations of high levels of Reynolds shear stress, enstrophy, and temperature fluctuations. The sublayer streaks seem to be passive and are often simply the rims of the indentation pockets arising from the turbulent–turbulent spots.

boundary layer | transition | turbulence | direct numerical simulation

The zero-pressure gradient, smooth, flat-plate boundary layer (ZPGSFPBL) is the simplest viscous external flow. It serves as the idealized limiting case and calibration benchmark of atmospheric and oceanic planetary boundary layers as well as aeronautical, maritime, and automotive boundary-layer flows. For over 60 y since the work by Theodorsen (1), a central theme in fundamental fluid mechanics research has been the search for the constitutive coherent structure in the turbulent ZPGSFPBL, particularly inside the near-wall/inner layer less than ∼100 viscous units away from the plate where the production and dissipation of turbulence kinetic energy reach their peaks (2–6). When the nature of the inner-layer structure and dynamics is thoroughly understood, this understanding can be incorporated in turbulence theory and predictive modeling.

Decades of research have produced an apparent consensus view (7–9) that the inner layer, which consists of the buffer layer and the viscous sublayer, of a turbulent ZPGSFPBL is populated by randomly distributed quasistreamwise vortices as well as elongated high- and low-momentum streaks. Streaks are thought to actively participate in a self-sustaining bursting cycle that includes streak generation, lift up, oscillation, breakdown, and streak regeneration. Theories have been developed to explain the mechanism of near-wall turbulence regeneration (10–13). However, many of these theories rely on direct numerical simulation (DNS) data of the internal fully developed channel or Couette flow rather than the external spatially developing ZPGSFPBL. Inner-layer theories of the turbulent ZPGSFPBL exist (14, 15) but are often based on the mostly 2D and coarse-resolution visualizations using dye/smoke or hydrogen bubble techniques as well as the inferred large-scale vortex motion (16, 17). Although the averaged geometric statistics of the streaks (spacing, width, and length scales) have been firmly established (2, 8), existing information on the dynamical aspects of the turbulent ZPGSFPBL streaks and their interaction with inner-layer vortex structures is far from being unequivocally clear. Given the coarse resolution and indirectness of much of the evidence and the degree of inference involved (16, 17), there is ample room to question whether the streak-centered cycle or the streak–vortex-centered mechanism is actually the most elementary turbulence regeneration process in the turbulent ZPGSFPBL or whether, perhaps, it is merely a symptom of a more fundamental underlying process.

Sustained efforts have been devoted to study properties and dynamics of transitional–turbulent spots (TRTSs) in the natural or bypass transitions of the ZPGSFPBL (18–22). It was long hoped that information extracted from TRTS during the inception of boundary-layer turbulence might shed light on the inner-layer dynamics, transport processes, and turbulence regeneration of the fully turbulent ZPGSFPBL. Although certainly logical and sensible, this objective has proven to be elusive, and research on TRTS has been rather firmly confined within the domain of boundary-layer transition.

A central question in the study of bypass transition in the narrow sense concerns the inception and growth mechanisms of

Significance

Uncovering the constitutive coherent structure in the inner layer of the canonical turbulent boundary layer has remained a central fluid mechanics theme, because it tests our intellectual ability to understand even the simplest external flow. We describe here how turbulent spots are initiated in bypass boundary-layer transition and uncover the ubiquity of concentrations of vortices in the fully turbulent region with characteristics remarkably like transitional–turbulent spots. We present strong evidence that these concentrations of vortices are the constitutive coherent structure of the inner layer near the wall. This study contributes to the unification of understanding of phenomena occurring in boundary-layer late-stage transition with near-wall turbulent boundary-layer structure and dynamics in the developed flow.

Author contributions: X.W. and P.M. designed research; X.W. performed research; P.M. contributed new reagents/analytic tools; X.W., J.M.W., J.S., and A.L.-D. analyzed data; J.-P.H. generated freestream inflow turbulence; and X.W., P.M., and J.M.W. wrote the paper.

Reviewers: J.K., University of California, Los Angeles; B.M., California Institute of Technology; and Ö.S., University of California, Berkeley.

Conflict of interest statement: A.L.-D. and Beverley McKeon are coauthors on a 2016 paper in the *Proceedings of the Center for Turbulence Research*. This paper documents preliminary results and is not an archival publication.

Freely available online through the PNAS open access option.

Data deposition: The data reported in this paper are at https://ctr.stanford.edu/research-data.

[1]To whom correspondence should be addressed. Email: moin@stanford.edu.

This article contains supporting information online at www.pnas.org/lookup/suppl/doi:10.1073/pnas.1704671114/-/DCSupplemental.

TRTS. By bypass transition in the narrow sense, we mean the superposition on a Blasius boundary layer by a continuous freestream flow of homogeneous isotropic turbulence (HIT) at an initial turbulence intensity of $1\sim4\%$. The flow so defined is a subclass of bypass transition in the general sense, which refers to laminar boundary-layer transition caused by finite amplitude perturbations arising from unrestricted sources, such as passing wakes, roughness, or blowing and suction (23). The prevailing view is that bypass transition in the narrow sense develops its own primary instability in the form of long streaks. The algebraic/transient growth of the streaks leads to a secondary instability, which occurs in the form of either streak meandering (24, 25) or streak interaction with freestream eddies (26).

By contrast, the idea put forward here is that the TRTS inception mechanism in bypass transition in the narrow sense is like the secondary instability that occurs in boundary-layer natural transition. Furthermore and importantly, we present evidence that the constitutive near-wall structure of the fully turbulent boundary layer is very similar to that of TRTS and that it can arise in much the same way.

Methods

In this work, we designed and executed a DNS of the spatially developing incompressible ZPGSFPBL from an initial laminar state through a well-controlled process of bypass transition in the narrow sense described above to the canonical fully turbulent state over a moderate Reynolds number range. Statistical characteristics of this ZPGSFPBL are presented in Figs. S1–S5 to validate that it is a faithful representation of this canonical flow case.

The DNS was performed on a mesh of $16{,}384\times500\times512$ grid points. The domain size is $21{,}563\theta_0\times2{,}250\theta_0\times844\theta_0$, where θ_0 is the inlet momentum thickness. The momentum thickness Reynolds number Re_θ develops from 80 to 3,000, with a corresponding decay of freestream turbulence (FST) intensity from 3 to 0.8% (Fig. S2) and a growth of the boundary-layer thickness δ from $7.55\theta_0$ to $312\theta_0$. $Re_\tau=u_\tau\delta/\nu$ reaches 1,003 at the exit, where u_τ is the friction velocity, and ν is the kinematic viscosity. Grid resolutions in wall-parallel planes are $3.5<\Delta x^+<5.5$ and $4.5<\Delta z^+<7$, respectively, where the superscript + denotes normalization with viscous scales. Measured using local values of the Kolmogorov length scale $\eta=(\nu^3/\varepsilon)^{1/4}$ at the station $Re_\theta=2{,}900$, the streamwise grid resolution ranges over $2<\Delta x/\eta<3$ for the inner layer and $0.5<\Delta x/\eta<2$ in the outer region. Along the wall-normal direction, the resolution is $0.4<\Delta y/\eta<2$ throughout the boundary layer. The inlet FST generation used the strong recycling methodology (27). Twenty-five independent temporally decaying HIT blocks were created using DNS following the approach of ref. 28. The velocity derivative skewness factor of the blocks is −0.47, and their longitudinal and transverse velocity correlation functions satisfy the relation from incompressible HIT theory. Ten random combination sets of 25 independent HIT blocks were created, and the resulting 250 blocks were sequentially aligned to form a narrow cuboid-shaped band of $211{,}000\theta_0\times844\theta_0\times844\theta_0$. At the inlet plane, the HIT band is aligned with the mean freestream, so that it is transported into the boundary-layer DNS domain at the mean freestream speed U_f. The lower edge of the band is located at $15\theta_0$ away from the plate to ensure that the inlet Blasius boundary layer is undistorted (29). In the freestream and very close to the inlet plane, when the front boundary of an incoming HIT block meets the trailing boundary of the previous one, discontinuity will arise in streamwise correlation functions. However, there is no detectable effect of this discontinuity on the velocity profiles inside the boundary layer (for example, the skin friction coefficient evolution in Fig. S2). Away from the inlet plane, this discontinuity fades away. Temperature is also included in the DNS at unit molecular Prandtl number. The nondimensional temperature φ is one at the wall and zero in the upper boundary following refs. 30 and 31. At the inlet, φ is prescribed using the Blasius laminar thermal boundary-layer profile without any fluctuations. Initial conditions are $u=1$, $v=w=0$, and $\varphi=0$. The time step of the DNS is $\Delta t=1.125\theta_0/U_f$. The incompressible Navier–Stokes equation and the continuity equation were solved using the fractional step method and the code of Pierce and Moin (32). After reaching a statistically steady state, the full velocity and temperature fields were saved at a rate of every $112.5\theta_0/U_f(100\Delta t)$ for a duration of $33{,}750\theta_0/U_f(30{,}000\Delta t)$. Each of these saved data files has a size of 203 GB. Data along four selected spanwise line bundles were also saved at every time step for a duration of $38{,}250\theta_0/U_f(34{,}000\Delta t)$. The four lines are located at $Re_\theta=670$ and 2,535 and the wall-normal positions of y/δ =0.05 and 0.5. Each bundle contains the selected line and its four immediate neighboring lines. Frequency spectra were computed by following the approach of ref. 33. The simulation was designed during the 2010 Center for Turbulence Research Summer Research Program at Stanford University, and the entire computation took nearly 5 calendar years to complete.

Results

In this numerical study, two previously unobserved phenomena were discovered. The first is that the FST perturbs the spanwise vortex lines inside the laminar Blasius boundary layer, producing strong, localized, spanwise vortices near the inlet. The spanwise vortex lines quickly kink and are subsequently lifted and stretched downstream into Λ vortices. They then evolve into hairpin packets of vortices (infant TRTS). This mechanism is analogous to the secondary instability of boundary-layer natural transition (34, 35). These TRTSs further evolve and mature, as they move downstream, where they infect surrounding low-speed streaks and cause them to meander and breakdown, resulting in a sudden spreading and growth of the existing TRTSs.

We also discovered that, downstream in the fully turbulent region of the simulation, spatially intermittent concentrations of small-scale vortices occur in the buffer-layer region and extend down to the wall. We call such inner-layer concentrations of vortices with high values of swirling strength λ_{ci}, the imaginary part of the complex eigenvalue of the velocity gradient tensor (9), turbulent–turbulent spots (TUTSs). TUTSs originate from hairpin packets in the turbulent boundary layer just as TRTSs do in the laminar to turbulent transition region. They are dynamically important for the generation of high levels of momentum and scalar transport. The discovery of TUTS inside the near-wall layer of the turbulent boundary layer bridges two previously segregated branches of study of the ZPGSFPBL, namely boundary-layer late-stage transition, which primarily focuses on TRTSs, and the inner-layer dynamics of the developed turbulent boundary layer, which until now, has been mostly concerned with the coupling of streaks and quasistreamwise vortices. Conditional statistics are similar in these two regions of the flow, as previously observed in ref. 36, along with the underlying constitutive flow structure.

TRTSs. Previous studies of bypass transition, in the narrow sense considered here, emphasized long meandering streaks that occupy a large percentage of the wall-normal dimension of the perturbed laminar boundary layer (24–26, 37). Although such streaks are present in this ZPGSFPBL during transition, it turns out, importantly, that, in our study, the long streaks occur downstream of the initiation of the dynamically significant Λ vortex structures (Fig. 1 and Movies S1 and S2). As shown in Fig. 1 and Movies S1 and S2, long-streak meandering does occur in our DNS with bypass transition, but it usually happens when the streak is strongly perturbed by a neighboring TRTS. The subsequent streak breakdown facilitates the spreading and growth of the existing spot, but it is not dynamically important in the inception of the TRTS. In natural transition, following the primary Tollmein–Schlichting wave instability, Λ vortices in various formation patterns (staggered, aligned, or mixed) emerge because of combined tilting and stretching of distorted spanwise vortex elements (the secondary instability) (38). Breakdown is ultimately caused by an inflectional instability, which often involves the generation of hairpin vortices (34, 35), and/or small-scale high-frequency fluctuations because of wrinkling of the high-shear layers associated with the Λ vortices (38). Here, as shown in Fig. 1 and Movies S1 and S2, Λ vortices develop from short quasispanwise vortex filaments instead of long streaks. Thus, the TRTS inception and laminar boundary-layer breakdown mechanism in this flow is analogous to the secondary instability of boundary-layer natural transition.

There is actually some literature suggesting this connection (39, 40) between natural transition and bypass transition. Klebanoff et al. (39) wrote that

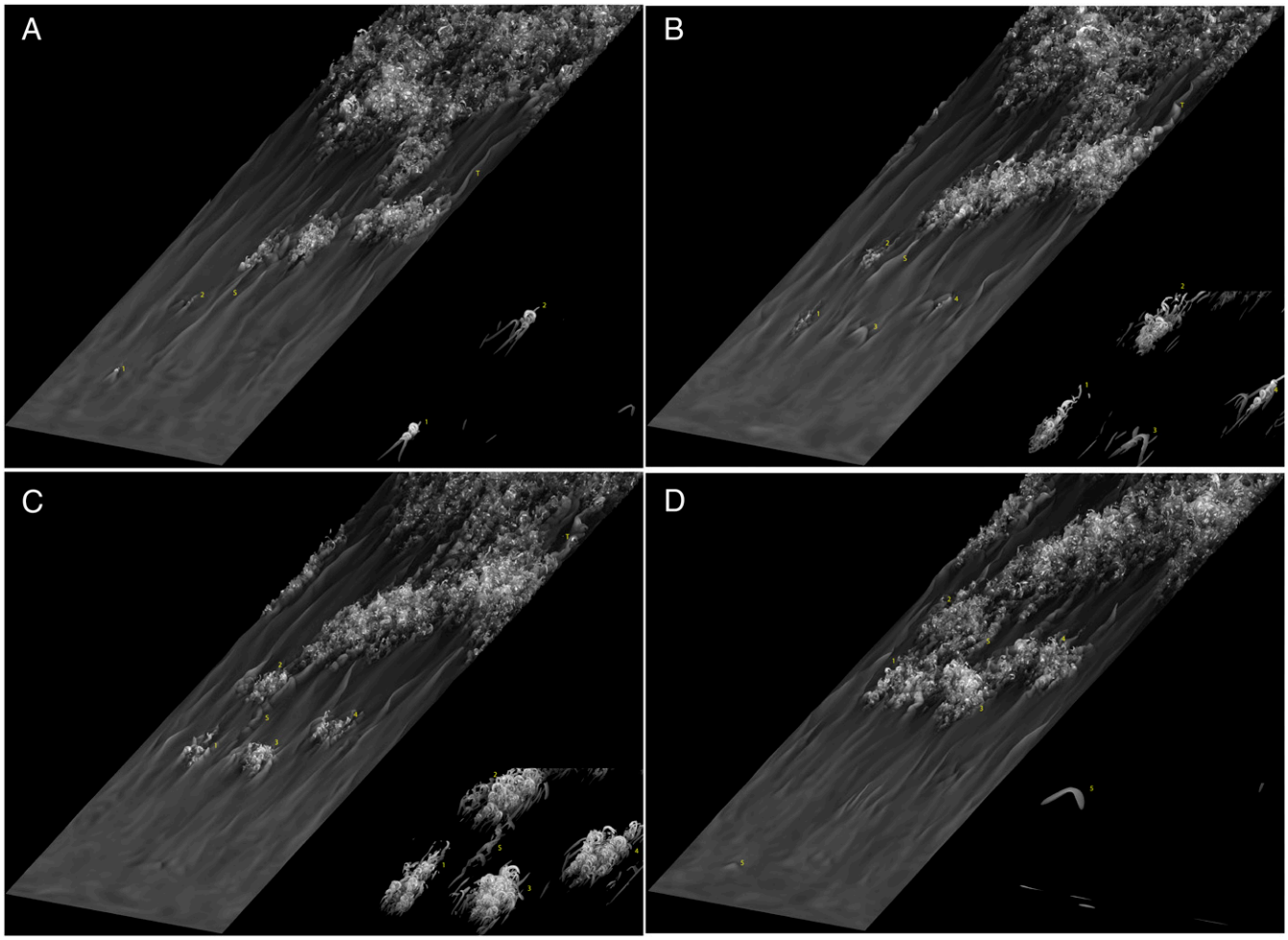

Fig. 1. Isosurface of temperature $\varphi = 0.25\varphi_{wall}$ in the transitional region $80 < Re_\theta < 450$ at four consecutive instances. *Insets* are the zoomed views of the isosurface of swirling strength $\lambda_{ci} = 22 \times 5.33 \times 10^{-4} U_f/\theta_0$. λ_{ci} is the imaginary part of the complex eigenvalue of the velocity gradient tensor (9). Grayscale represents local values of y/δ with bright white color corresponding to $y/\delta \geq 1$. Instances (*A*) $t = 112{,}000\Delta t$, (*B*) $t = 112{,}600\Delta t$, (*C*) $t = 113{,}100\Delta t$, and (*D*) $t = 113{,}900\Delta t$. Labels 1–5 mark five TRTSs; labels S and T mark two meandering streaks. It is evident that the infant TRTS is caused by a Λ vortex originating from a spanwise vortex filament. The meandering and breakdown of long streaks occur later when the streaks are contaminated by existing neighboring TRTSs, which in turn, provides a means for the existing spots to grow in size.

> Increasing the ribbon amplitude had no significant effects on the character of the wave generated except to move the point of departure and breakdown further upstream. With sufficiently large amplitude, it was possible to "bypass" the linear TS-wave range completely. This was graphically demonstrated by observing the behavior of a wave of such frequency that it should damp according to the linear theory. At low amplitudes the wave damped as expected, but at sufficiently high amplitude it did not damp and very rapidly led to breakdown of laminar flow "in much the same manner" as a wave within the amplified zone.

Their statement is remarkable and particularly relevant here, because they semiexplicitly equated the bypass transition mechanism with the secondary instability of natural transition. The statement is further interesting, because it seems to us that this was the first time that the descriptor "bypass" appeared in an archival journal within the context of boundary-layer transition.

Based on early experimental visualizations, ref. 19 conjectured that the constitutive structure of TRTSs is a large horseshoe vortex with small-scale vortices superimposed on its arc. Fig. 1, Fig. S6, and Movie S1 show that actually infant/young TRTSs are hairpin packets and that more matured ones are local concentrations of hairpin vortices and random vortex filaments. The structure of the turbulence within TRTS was also commented on by Gad-el-Hak et al. (20) based on their laser-induced fluorescence visualization. Although they were not able to fully view the three-dimensionality of the vortices, they did observe what they described as individual eddies in the interior of the spots. Furthermore, they noticed that the spots grow laterally in the wall-parallel direction much more rapidly than in the wall-normal direction. This lateral growth they attributed to destabilization of the surrounding flow, consistent with our observation of the TRTS destabilization of the surrounding streaks.

The initiation of the TRTS in our simulation is quite different from the streak instability mechanism of bypass transition described in refs. 24–26 and 37. As discussed above, during the bypass transition of this study, the instability of streaks caused by excitation and contamination of nearby TRTS occurs after the spots have already been created, and it only contributes to the growth of the existing TRTS.

TUTSs. To clearly visualize and identify the inner-layer structures in the developed region of the flow, in Fig. 2, only the first 120 grid planes above the wall are shown, with the flow above made invisible. This near-wall layer corresponds roughly to $y < 0.15\delta$ or $y^+ < 120$ over the range $2{,}500 < Re_\theta < 2{,}900$. In this region, TUTSs are numerous, and they are not limited to the

particular instances and locations of Fig. 2*A* (Fig. S7 and Movies S3 and S4). The shapes of the TUTS can be broadly divided into two categories: oval patch-like structures and stripe packet-like structures. Some of the spots display a visible arrowhead shape during certain stages of their development. These TUTSs are in many ways similar to the TRTSs in Fig. 1, Fig. S6, and Movie S1. Infant and young spots are hairpin vortex packets, whereas more mature spots are a mix of hairpin vortices and what appear to be random vortex filaments. Because TUTSs exist inside a more chaotic environment deep inside the turbulent boundary layer, they contain more random filaments. Nevertheless, they can be readily identified as distinct coherent structures. The TUTSs are dynamically important for near-wall turbulence production and transport processes. The spatial and temporal coordinates of TUTS coincide with concentrations of very high levels of Reynolds shear stress, temperature fluctuations, and enstrophy as seen in Fig. S8, the space–time coordinates of which are correlated with Fig. 2. Note in Fig. S8 the high degree of temporal intermittency of the enstrophy signal. Movie S4 suggests that the length and width of those easily identifiable TUTSs are $\sim 1\,\delta$ and $0.3\,\delta$ or 1,000 and 300 wall units, respectively. Note that the spanwise dimension of the computational domain is roughly 3δ at this Reynolds number range.

It is logical to inquire whether the observed TUTSs are transported from the upstream transitional region and thus, simply the remnants of the TRTSs. In fact, we found that these TUTSs are generated locally within the viscous sublayer and the buffer layer of the turbulent ZPGSFPBL. Fig. 3 presents snapshots of a TUTS from its infancy to maturity within the range $2{,}700 < Re_\theta < 2{,}800$. It is seen that the infant TUTS is initiated from a weak hairpin packet wrapped around the leg elements of an existing hairpin vortex. The infant TUTS subsequently grows into a new long hairpin packet mixed with random filaments followed by additional development into a mature TUTS. This process is consistent with the hairpin vortex autoregeneration mechanism advanced in refs. 4 and 6. Many, but not all, TUTSs can be traced to their origin, like the one in Fig. 3. Where such tracing is not possible, it is usually because of the complicated merging and splitting of matured TUTSs (Movie S4). In Movie S5, spots in the transitional and turbulent regions are compared and traced backward in time. It is seen there that the mature spots have evolved from small hairpin packets in both flow regions. Based on visualization, over the range $2{,}000 < Re_\theta < 3{,}000$, the small individual hairpin vortices inside the TUTS have rather short lifespans, usually disappearing within a distance of $1\,\delta$ or approximately 1,000 wall units. However, the coherence of a TUTS as an entity has a much longer duration, typically on the order of 6δ, before it either fades away, splits, or merges with another TUTS. Lifetime statistics of the TUTS are not extracted in this study.

At lower visualization threshold levels of isosurfaces of λ_{ci}, the wall-layer TUTSs are surrounded and even somewhat shrouded by other vortex structures with weaker swirling strength, but the spots themselves are discernable even in the presence of surrounding noise because of the strong inner-layer spatial intermittency. With progressively increasing levels of λ_{ci}, the weaker vortex structures gradually fade from view, thus making the TUTSs more distinct. Movie S6 documents this process.

Viscous sublayer streaks have received much attention in turbulent boundary-layer structure research. We visualize these streaks using temperature isosurfaces, which are analogous to dye or smoke released from the plate in experiments. With the assigned temperature boundary condition, a ridge in the isosurface of φ provides a 3D view of a low-momentum streak. Fig. 2*B* shows the isosurface of $\varphi = 0.95$ at $t = 132{,}300\theta_0/U_f$ and for the spatial range $2{,}400 < Re_\theta < 2{,}650$, where the bright white color indicates $y^+ \approx 4$. Previous literature using 2D streamwise velocity or temperature contours seems to suggest that the viscous sublayer streaks are smoothly meandering narrow stripes. It is thus surprising to observe in Fig. 2*B* and Movie S3 that many of the sublayer streaks are severely indented/scarred instead of being smooth and that streaks are terminated in regions where concentrated indentations are present. It is also evident that many of the sublayer streaks themselves are actually the rims of the indentation

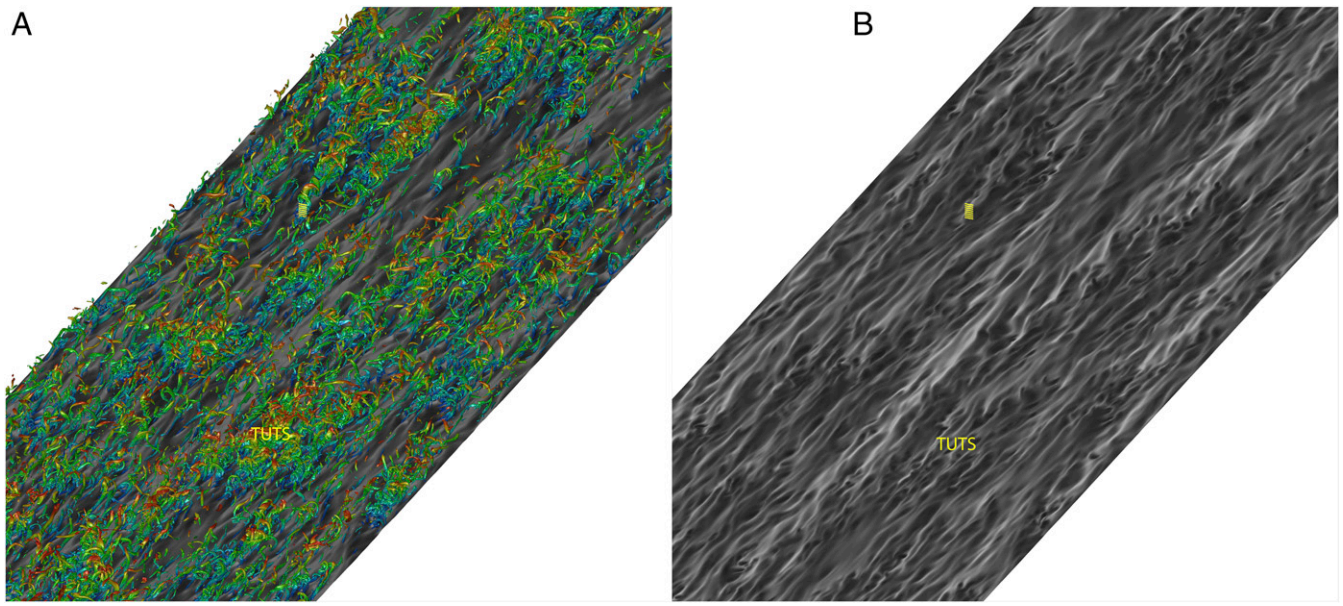

Fig. 2. TUTSs and viscous sublayer streaks over the range $2{,}400 < Re_\theta < 2{,}650$ at instance $t = 117{,}600\Delta t$. (*A*) Swirling strength $\lambda_{ci} = 35 \times 5.33 \times 10^{-4} U_f/\theta_0$ overlaid on the temperature isosurface of *B*. Blue indicates $y^+ < 25$; red corresponds to $100 < y^+ < 125$. (*B*) Temperature isosurface $\varphi = 0.95\varphi_{wall}$. Bright color indicates higher wall-normal distance that is always less than $y^+ = 5$. Each ridge in the temperature isosurface corresponds to a low-momentum streak. It is evident that the sublayer streaks are indented, segmented, and terminated by the TUTSs, and the sublayer streaks are often simply the edges of indentation pockets arising from the spots. The small yellow bars mark the *x* and *z* coordinates for the time history signal processing in Fig. S8. The label TUTS marks one of the TUTSs.

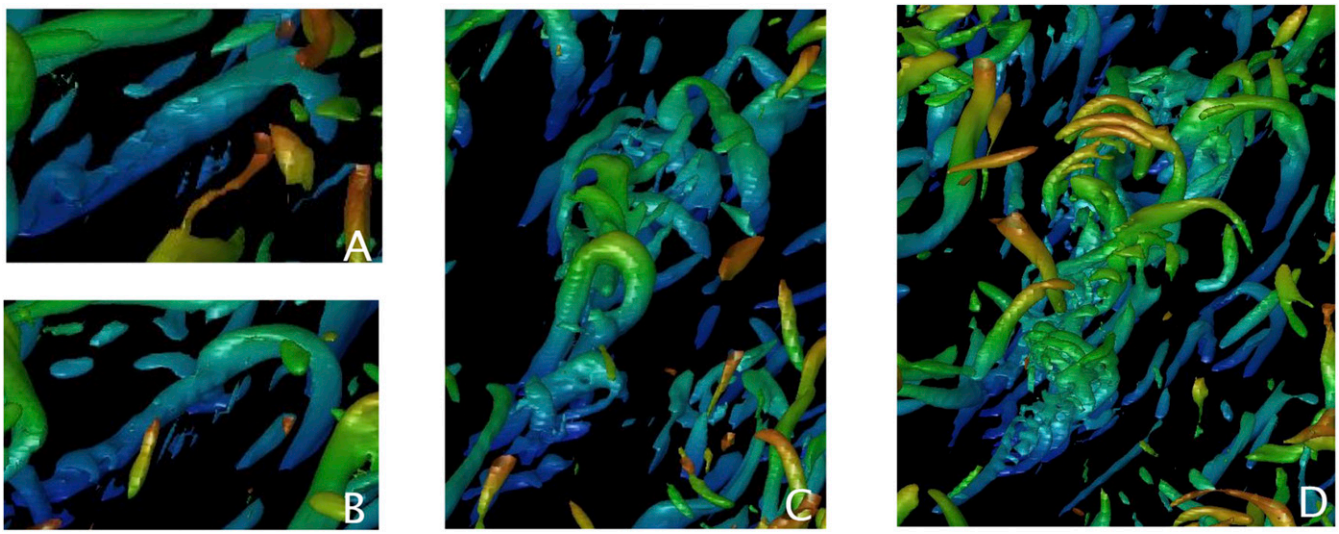

Fig. 3. Zoomed views of the isosurface of swirling strength $\lambda_{ci} = 35 \times 5.33 \times 10^{-4} U_f/\theta_0$ showing the inception and development of one TUTS over the range $2{,}700 < Re_\theta < 2{,}800$. Blue indicates $y^+ < 25$, green corresponds to $25 < y^+ < 50$, and yellow corresponds to $50 < y^+ < 75$. At instances (*A*) $t = 118{,}100\Delta t$, (*B*) $t = 118{,}200\Delta t$, (*C*) $t = 119{,}000\Delta t$, and (*D*) $t = 119{,}300\Delta t$. It is evident that the infant TUTS is a weak hairpin packet wrapped around the leg element of a previous generation hairpin vortex. It grows into a new long hairpin packet mixed with random filaments followed by additional development into a mature TUTS.

pockets. Our results also show that sublayer streaks are not persistent. They are short-lived and usually cannot be traced beyond 50 viscous time units. Pockets (void of smoke) were observed earlier by Falco (5). Corino and Brodkey (3) noted that the viscous sublayer streaks are continuously disturbed by small-scale velocity fluctuations of low magnitude, and they are periodically disturbed by fluid elements that penetrated into the region from positions further removed from the wall.

Prompted by the recent study (41), which showed that, in spatially developing pipe flow transition, the otherwise axisymmetric isosurface of the passive scalar is indented by hairpin packets, in Fig. 2*A* and Movie S4, we have overlaid the isosurfaces of swirling strength, λ_{ci}, on top of the temperature isosurfaces of Fig. 2*B* and Movie S3, respectively. Sublayer streak termination occurs at the locations of the TUTSs, which as described above, are spatial concentrations of small-scale vortices across the buffer region with high values of λ_{ci}. It is quite obvious from Fig. 2 and Movies S3 and S4 that the sublayer streaks appear to be rather passive, and they are strongly affected by the large-scale TUTS. Note that here the vortex height can be inferred from Fig. 2 as the isosurface of λ_{ci} is colored by local values of y/δ.

A composite high-resolution and long-duration version of the movies can be downloaded at the Stanford Center for Turbulence Research website (https://ctr.stanford.edu/research-data) together with boundary-layer statistics. Much of the turbulent ZPGSFPBL theory development over the past four decades has been based on the 2D and coarse-resolution visualizations using dye/smoke or hydrogen bubble techniques as well as the inferred large-scale vortex motion (2, 5, 16, 17). This composite movie provides unprecedented fine details on ZPGSFPBL near-wall vortex dynamics with long temporal duration and large spatial coverage. The movie also includes detailed vortex structures at the boundary layer turbulence and freestream turbulence interface (BTFTI).

Quantification of TRTS and TUTS Properties. The turbulence in the inner region is remarkably spatially intermittent, occurring primarily in concentrated spots surrounded by very low levels of swirling strength. At $y^+ = 50$, for example, 33% of the plane has nearly zero swirling strength in the developed turbulence region of $2{,}100 < Re_\theta < 2{,}860$ compared with 32% in the transition region of $150 < Re_\theta < 350$ in the same y^+ plane. In the developed turbulence region for this $y^+ = 50$ plane, Fig. 4*A* shows that about 80% of the total swirling strength, λ_{ci}, is at or above a threshold of $\alpha \sim 2.2$, but this level of swirling strength only occupies about 40% of the total plane. The threshold α is defined as $\lambda_{ci}/\langle\lambda_{ci}\rangle$, where $\langle\lambda_{ci}\rangle$ is the mean swirling strength in the plane. When Fig. 4*A* is compared with Fig. 4*B* for the transition region at the same y^+ plane, similar percentages are observed for $\alpha \sim 1.2$. It is evident that this spatial intermittency of the developed turbulence is quite similar to that of the transitional flow. Furthermore, these types of plots for other wall-parallel planes in the inner layer for both the developed turbulence and transitional regions of the flow show this same similarity.

This strong spatial intermittency of the developed flow turbulence is further shown in Fig. S9*A*. There, the probability density function (PDF) of λ_{ci} for $y^+ = 50$ is compared with the PDF of λ_{ci} for the transitional region in Fig. S9*B*, both plotted as functions of the threshold α defined above. In both cases, the left-most bins have the highest probability, because they contain all of the zero values of λ_{ci}. To the right of these left-most bins, the probabilities drop dramatically and then rise to second maxima at λ_{ci} values near the mean in both cases. Both of these PDFs have long tails, indicating the infrequent very high values of λ_{ci} that occur within the cores of the TUTSs and TRTSs. PDFs of other inner-layer planes display the same evidence of strong spatial intermittency, indicating that the concentrated spots of turbulence in the developed flow are very much like the transition spots.

The birthrates of large new TRTSs and TUTSs are shown in Fig. 5. These spots, with streamwise lengths greater than $50\theta_0$, are identified with the connectivity algorithm of ref. 42, and they are traced back in time and space to their origins, as visualized in Movie S5, using the methodology of ref. 43. The number of new spots per unit area of the inlet momentum thickness θ_0^2 are plotted for both the transitional and developed turbulence regions. As the Reynolds number increases in the transitional region, the number density of the spots grows as expected. After the turbulence reaches a developed state, the number saturates at a value of about 40×10^{-6}, which suggests that new spots are born at a constant rate of a little over one spot per area of $160\theta_0 \times 160\theta_0$. Movie S5 and Fig. S10 make clear that the hairpin packets from which the TUTSs evolve in the developed flow are similar to those in the transitional flow and that these TUTSs are

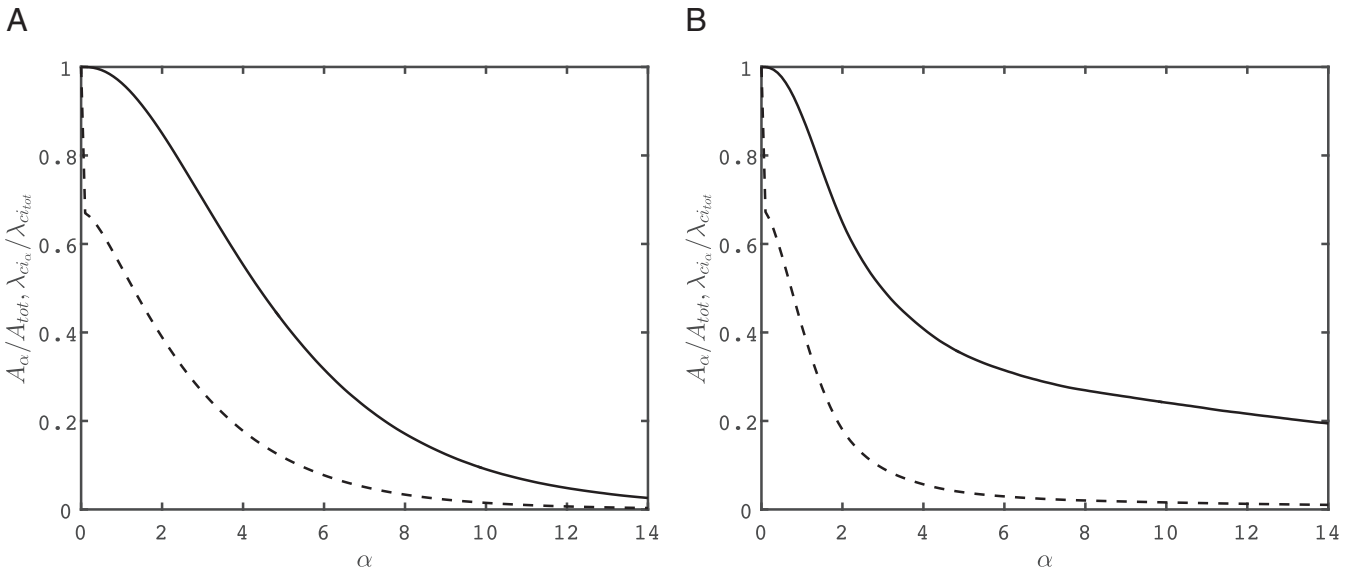

Fig. 4. For $y^+ = 50$ in (*A*) the developed turbulence region of $2{,}100 < Re_\theta < 2{,}860$ and (*B*) the transitional flow region of $150 < Re_\theta < 350$, the fraction of the total swirling strength (solid line), λ_{ci}, was compared with the fraction of the plane (dashed line) occupied by this swirling strength for a given threshold α. The threshold α is defined as $\lambda_{ci}/<\lambda_{ci}>$, where $<\lambda_{ci}>$ is the mean swirling strength in the plane. About 80% of the total swirling strength occurs in only about 40% of the area of this plane in the inner layer at $\alpha \sim 2.2$ for the developed turbulence region and $\alpha \sim 1.2$ for the transition region. Similar percentages were found for other inner-layer wall-parallel planes. This similarity shows that the spatial intermittency of the developed turbulence is quite similar to that of the transitional flow.

not remnants of transition. On the contrary, they are born in the developed turbulence region.

Relationship of TUTSs to Previous Investigations. The question arises about how the TUTSs in the fully turbulent boundary layer described here relate to previous work. Using an ensemble average picture of the TRTS, refs. 44 and 45 hypothesized that the large-scale motions (LSMs) of the turbulent ZPGSFPBL are large horseshoe vortices superimposed with small-scale fluctuations. Delo et al. (46) related turbulent ZPGSFPBL momentum transport to a TRTS model. However, none of these investigations detected spatially intermittent concentrations of small-scale vortices of high swirling strength in the inner layer of the turbulent ZPGSFPBL (i.e., TUTSs), with characteristics similar to those of TRTSs.

Park et al. (36) compared statistics, including vorticity, dissipation rate, and octant classified momentum and heat fluxes, conditionally sampled from TRTSs with those from the downstream fully turbulent region of the ZPGSFPBL. They found that the compared statistics were remarkably similar in both flow regions, suggesting albeit indirectly, that there exists a strong statistical similarity between the processes involved in the inception and transport processes of boundary-layer turbulence in transition and the regeneration and transport processes of the fully turbulent ZPGSFPBL. However, until this work, it seems that there has been no direct evidence to structurally connect TRTS with the inner-layer structure and dynamics of the fully turbulent ZPGSFPBL.

Ref. 47 also studied concentration of vortices, termed as vortex clusters, in periodic turbulent channel flows. The authors found two classes: detached clusters that are small, short-lived, and roughly homogeneous and isotropic and attached ones that are rooted near the wall (below $y^+ \sim 20$) and associated with wall-normal momentum transport. Still, the main focus of ref. 47 was vortex clusters extending far from wall, and possible connections between the dynamics of these structures in the transitional and turbulent regions were not considered.

As mentioned above, in their early manifestations, infant and young TUTSs are hairpin packets much like those described by Adrian et al. (6) and Adrian (9). In this sense, there is a strong connection between the TUTSs and the work of Adrian et al. (6). They describe the "nesting" of younger, smaller packets within larger, older packets. However, their 2D experimental data did not permit them to make observations or conjectures about how these younger, smaller packets in and below the buffer layer can agglomerate into the TUTSs that we observe in our investigation or how this process is analogous to the agglomeration of hairpin

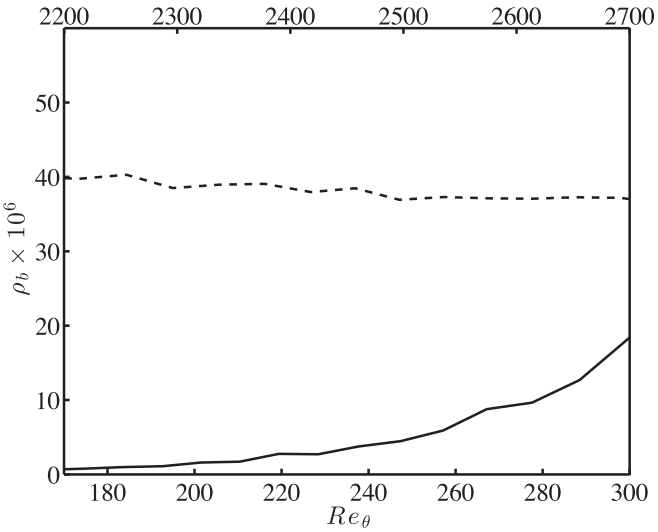

Fig. 5. Birthrates of new TRTSs (solid line and bottom horizontal axis) and TUTSs (dashed line and top horizontal axis). Large spots with streamwise lengths greater than $50\theta_0$ were identified for this figure with the connectivity algorithm of ref. 42. They are traced back in time and space to their origins as also visualized in Movie S5. The number of new spots per unit area of the inlet momentum thickness θ_0^2 is plotted for both the transitional and developed turbulence regions. As the Reynolds number increases in the transitional region, the number density of the spots grows as expected, and it eventually saturates in the developed flow region at a value of about 40×10^{-6}. Thus, new spots are born at a constant rate of a little over one spot per area of $160\theta_0 \times 160\theta_0$ after the turbulence reaches a developed state.

packets into matured TRTSs during transition. Both in transition and the fully turbulent boundary layer, these agglomerations into spots are spatially intermittent. Hairpin packet spatial intermittency was somewhat suggested in ref. 48.

In a very recent paper, Jodai and Elsinga (49) have observed hairpin packets in the buffer layer of their experimental turbulent ZPGSFPBL using high-spatial and -temporal resolution tomographic particle image velocimetry (PIV). Furthermore, they have been able to study the local generation and evolution of new hairpin vortices connected to these packets, showing that the hairpins were not convected downstream from the transitional region. Our DNS has uncovered these near-wall hairpin packets as well and shown that they grow and agglomerate into what we are calling TUTSs that occupy the region of the flow from just above the buffer layer all of the way down to the wall and furthermore, that they are distinct and thus, spatially intermittent in this region.

The Reynolds number range covered in this study, $80 < Re_\theta < 3{,}000$, is only moderate but nevertheless, larger than the set of discrete values within the range of $545 < Re_\theta < 2{,}060$ used in the classical turbulent boundary-layer streak bursting experiments of Kline and coworkers (2, 16, 17). The three aforementioned more recent PIV experiments (6, 48, 49) were performed in turbulent ZPGSFPBLs at $2{,}000 < Re_\theta < 3{,}000$, also overlapping with our DNS Reynolds number range. Tennekes and Lumley (50) argued that, in the inertial sublayer of high Reynolds number wall-bounded flows, the Reynolds shear stress asymptotes to ρu_τ^2, and the mean velocity gradient is approximately $u_\tau/\kappa y$. This approximation leads to a turbulence production rate of $u_\tau^3/\kappa y$, which is further assumed to be balanced by the viscous dissipation rate ε for high Reynolds number equilibrium wall-bounded flows. In Fig. S1*B*, it is seen that this dissipation rate is in excellent agreement with the asymptotic argument of ref. 50. This agreement suggests that this turbulent boundary layer under a mild FST is a statistically representative, canonical ZPGSFPBL and that it is in overall equilibrium. It also suggests that there may not be much substantial difference between a canonical turbulent ZPGSFPBL at moderate Reynolds number ($2{,}000 < Re_\theta < 3{,}000$) and that at a much higher Reynolds number, notwithstanding the expanded range of eddy scales in the latter evidenced by the appearance of a second peak in the streamwise velocity spectrum (51).

These dynamically important TUTSs described herein for the inner layer ($y^+ < \sim 100$) are structurally similar to TRTSs. The inception process of our TUTS seems to agree more with the parent–offspring autoregeneration mechanism (52, 53) than the streak–vortex self-sustaining cycle theory (10, 54–56). Fig. 2 and Fig. S7 show that the boundary-layer viscous sublayer streaks are subjected to the indentation and disruption by the TUTS; some of the streaks are simply the rims of the TUTS. At this point, we are unable to entirely rule out the possibility that the streak–vortex self-sustaining cycle mechanism could also be a potential factor at play in this flow, coexisting with the TUTS mechanism. These observations regarding the passive nature of the streaks vs. the more dominating active role of the TUTS seem to be at odds with the observations of Kline and coworkers (2, 16, 17), who reported that the dye/smoke was scooped up, presumably by a vortex, and then went through a violent breakup process. Our view is that the smoke lift up, oscillation, and breakup may be a by-product of the TUTS dynamics. The coarse-resolution studies of refs. 2, 16, and 17 did not permit those authors to detect the vortical structure responsible for their observations on the dye/smoke. Furthermore, we found that buffer-layer streak images, extracted using the isosurface of $\varphi = 0.75$, are very similar in terms of geometrical characteristics and connection with the TUTS to the sublayer streak images extracted using $\varphi = 0.95$ as in Fig. 2*B* and Fig. S7*B*. Thus, both the viscous sublayer streaks and the buffer-layer streaks are passive in relation to the TUTS. The similarity between these two types of streaks was also identified in previous studies.

These TUTSs are only the lowest level in a hierarchy of structures contained in a turbulent ZPGSFPBL (4–6, 9). Other higher-level and larger-scale structures in the hierarchy (57–59) are not the focus of this paper. However, we note that the wake region $(0.5 < y/\delta < 1)$ and the BTFTI region are densely populated by groves of concentrated large-scale hairpin vortices (Movie S7). The space between the neighboring groves forms the deep valleys observed frequently from previous smoke visualizations of LSMs (5, 9) in turbulent ZPGSFPBL. At this stage, it is unclear whether the inception of TUTS is aided by perturbations arising from the deep penetration of outer freestream flow into the inner layer. Nevertheless, we emphasize that one hallmark of the turbulent ZPGSFPBL is the deep penetration of freestream irrotational flow or freestream turbulence into the inner layer. This feature is absent in the periodic channel or Couette flow. This distinguishing characteristic perhaps holds the key in reconciling these observations in the ZPGSFPBL with the existing streak–vortex-centered theories developed using the channel and Couette flow, although this is purely a conjecture for now.

The experimental results of ref. 60 suggest that the log-layer large-scale motions modulate the near-wall small-scale fluctuations. Although the modulation of the small-scale inner-layer turbulence by the large outer-layer scales is not the focus of this investigation, it is nevertheless worth pointing out that the TUTSs revealed in our study extend from the wall to (at least) the lower logarithmic region, a fact consistent with the modulation observation. Notwithstanding the moderate Reynolds number achieved in our DNS, this high-resolution, long-temporal duration, and large spatial extent database provides a reliable venue to address this issue and other outstanding issues.

Finally, it is important to remark that our observations suggest that TUTSs are promising candidates to act as fundamental building blocks of wall-bounded turbulence. This identification is a significant result, because understanding the physics of this elemental flow unit will provide insight into the self-sustaining mechanism of wall turbulence.

ACKNOWLEDGMENTS. X.W. and J.-P.H. acknowledge support from the Natural Science and Engineering Research Council of Canada. P.M. thanks the US Department of Energy and Air Force Office of Scientific Research for support. J.M.W. acknowledges support from the University of Maryland Burgers Program for Fluid Dynamics. J.S. and A.L-D. are supported by the Center for Turbulence Research at Stanford University.

1. Theodorsen T (1952) Mechanism of turbulence. *Proceedings of the Midwestern Conference on Fluid Mechanics* (Ohio State Univ, Columbus, OH), pp 1–18.
2. Kline SJ, Reynolds WC, Schraub FA, Runstadler PW (1967) The structure of turbulent boundary layers. *J Fluid Mech* 30:741–773.
3. Corino ER, Brodkey RS (1969) A visual investigation of the wall region in turbulent flow. *J Fluid Mech* 37:1–30.
4. Smith CR, Walker JDA, Haidari AH, Sobrun U (1991) On the dynamics of near-wall turbulence. *Philos Trans A Math Phys Eng Sci* 336:131–175.
5. Falco RE (1991) A coherent structure model of the turbulent boundary layer and its ability to predict Reynolds number dependence. *Philos Trans A Math Phys Eng Sci* 336: 103–129.
6. Adrian RJ, Meinhart CD, Tomkins CD (2000) Vortex organization in the outer region of the turbulent boundary layer. *J Fluid Mech* 422:1–54.
7. Cantwell BJ (1981) Organized motion in turbulent flow. *Annu Rev Fluid Mech* 13:457–515.
8. Robinson SK (1991) Coherent motions in the turbulent boundary layer. *Annu Rev Fluid Mech* 23:601–639.
9. Adrian RJ (2007) Hairpin vortex organization in wall turbulence. *Phys Fluids (1994)* 19: 041301.
10. Hamilton JM, Kim J, Waleffe F (1995) Regeneration mechanisms of near-wall turbulence structures. *J Fluid Mech* 287:315–348.
11. Schoppa W, Hussain F (2002) Coherent structure generation in near-wall turbulence. *J Fluid Mech* 453:57–108.
12. Jiménez J, Pinelli A (1999) The autonomous cycle of near-wall turbulence. *J Fluid Mech* 389:335–359.
13. McKeon BJ, Sharma AS (2010) A critical-layer framework for turbulent pipe flow. *J Fluid Mech* 658:336–382.
14. Aubry N, Holmes P, Lumley JL, Stone E (1988) The dynamics of coherent structures in the wall region of a turbulent boundary layer. *J Fluid Mech* 192:115–173.

15. Carpenter PW, Kudar KL, Ali R, Sen PK, Davies C (2007) A deterministic model for the sublayer streaks in turbulent boundary layers for application to flow control. *Philos Trans A Math Phys Eng Sci* 365:2419–2441.
16. Offen GR, Kline SJ (1974) Combined dye-streak and hydrogen-bubble visual observations of a turbulent boundary layer. *J Fluid Mech* 62:223–239.
17. Offen GR, Kline SJ (1975) A proposed model of the bursting process in turbulent boundary layers. *J Fluid Mech* 70:209–228.
18. Wygnanski I, Sokolov M, Friedman D (1976) On a turbulent spot in a laminar boundary layer. *J Fluid Mech* 78:785–819.
19. Cantwell B, Coles D, Dimotakis P (1978) Structure and entrainment in the plane of symmetry of a turbulent spot. *J Fluid Mech* 87:641–672.
20. Gad-el-Hak M, Blackwelder RF, Riley JJ (1981) On the growth of turbulent regions in laminar boundary layers. *J Fluid Mech* 110:73–95.
21. Perry AE, Lim TT, Teh EW (1981) A visual study of turbulent spots. *J Fluid Mech* 104: 387–405.
22. Singer BA, Joslin RD (1994) Metamorphosis of a hairpin vortex into a young turbulent spot. *Phys Fluids (1994)* 6:3724–3736.
23. Wu X, Moin P, Hickey J-P (2014) Boundary layer bypass transition. *Phys Fluids (1994)* 26:091104.
24. Hack MJ, Zaki T (2016) Data-enabled prediction of streak breakdown in pressure-gradient boundary layers. *J Fluid Mech* 801:43–64.
25. Schlatter P, Brandt L, de Lange HC, Henningson DS (2008) On streak breakdown in bypass transition. *Phys Fluids (1994)* 20:101505.
26. Durbin P, Wu X (2007) Transition beneath vortical disturbances. *Annu Rev Fluid Mech* 39:107–128.
27. Wu X (2017) Inflow turbulence generation methods. *Annu Rev Fluid Mech* 49:23–49.
28. Mansour NN, Wray AA (1994) Decay of isotropic turbulence at low Reynolds number. *Phys Fluids (1994)* 6:808–814.
29. Wu X, Moin P (2009) Direct numerical simulation of turbulence in a nominally zero-pressure-gradient flat-plate boundary layer. *J Fluid Mech* 630:5–41.
30. Wu X, Moin P (2010) Transitional and turbulent boundary layer with heat transfer. *Phys Fluids (1994)* 22:085105.
31. Wu X (2010) Establishing the generality of three phenomena using a boundary layer with freestream passing wakes. *J Fluid Mech* 664:193–219.
32. Pierce CD, Moin P (2004) Progress variable approach for large-eddy simulation of non-premixed turbulent combustion. *J Fluid Mech* 504:73–97.
33. Choi H, Moin P (1990) On the space-time characteristics of wall-pressure fluctuations. *Phys Fluids A Fluid Dyn* 2:1450–1460.
34. Bake S, Meyer DG, Rist U (2002) Turbulence mechanism in Klebanoff transition: A quantitative comparison of experiment and direct numerical simulation. *J Fluid Mech* 459:217–243.
35. Sayadi T, Hamman CW, Moin P (2013) Direct numerical simulation of complete H-type and K-type transitions with implications for the dynamics of turbulent boundary layers. *J Fluid Mech* 724:480–509.
36. Park GI, Wallace JM, Wu X, Moin P (2012) Boundary layer turbulence in transitional and developed states. *Phys Fluids (1994)* 24:035105.
37. Matsubara M, Alfredsson PH (2001) Disturbance growth in boundary layers subjected to freestream turbulence. *J Fluid Mech* 430:149–168.
38. Herbert T (1988) Secondary instability of boundary layers. *Annu Rev Fluid Mech* 20: 487–526.
39. Klebanoff PS, Tidstrom KD, Sargent LM (1962) The three-dimensional nature of boundary layer instability. *J Fluid Mech* 12:1–34.
40. Ovchinnikov V, Choudhari MM, Piomelli U (2008) Numerical simulations of boundary layer bypass transition due to high-amplitude freestream turbulence. *J Fluid Mech* 613:135–169.
41. Wu X, Moin P, Adrian RJ, Baltzer JR (2015) Osborne Reynolds pipe flow: Direct simulation from laminar through gradual transition to fully developed turbulence. *Proc Natl Acad Sci USA* 112:7920–7924.
42. Lozano-Durán A, Flores O, Jiménez J (2012) The three-dimensional structure of momentum transfer in turbulent channels. *J Fluid Mech* 694:100–130.
43. Lozano-Durán A, Jiménez J (2014) Time-resolved evolution of coherent structures in turbulent channels: Characterizations of eddies and cascades. *J Fluid Mech* 759: 432–471.
44. Brown GL, Thomas ASW (1977) Large structure in a turbulent boundary layer. *Phys Fluids (1994)* 20:S243–S252.
45. Savas Ö, Coles D (1985) Coherence measurements in synthetic turbulent boundary layers. *J Fluid Mech* 160:421–446.
46. Delo CJ, Kelso RM, Smits AJ (2004) Three-dimensional structure of a low-Reynolds-number turbulent boundary layer. *J Fluid Mech* 512:47–83.
47. del Álamo J, Jiménez J, Zandonade P, Moser RD (2006) Self-similar vortex clusters in the turbulent logarithmic region. *J Fluid Mech* 561:329–358.
48. Ganapathisubramani B, Longmire EK, Marusic I (2003) Characteristics of vortex packets in turbulent boundary layers. *J Fluid Mech* 478:35–46.
49. Jodai Y, Elsinga GE (2016) Experimental observation of hairpin auto-generation events in a turbulent boundary layer. *J Fluid Mech* 795:611–633.
50. Tennekes H, Lumley JL (1972) *A First Course in Turbulence* (MIT Press, Cambridge, MA).
51. Smits AJ, McKeon BJ, Marusic I (2011) High-Reynolds number wall turbulence. *Annu Rev Fluid Mech* 43:353–375.
52. Zhou J, Adrian RJ, Balachandar S, Kendall TM (1999) Mechanisms for generating coherent packets of hairpin vortices in channel. *J Fluid Mech* 387:353–396.
53. Panton RL (2001) Overview of the self-sustaining mechanisms of wall turbulence. *Prog Aerosp Sci* 37:341–383.
54. Waleffe F (1997) On a self-sustaining process in shear flows. *Phys Fluids (1994)* 9: 883–900.
55. Hwang Y, Bengana Y (2016) Self-sustaining process of minimal attached eddies in turbulent channel flow. *J Fluid Mech* 795:708–738.
56. Farrell BF, et al. (2016) A statistical state dynamics-based study of the structure and mechanism of large-scale motions in plane Pioseuille flow. *J Fluid Mech* 809:290–315.
57. Hutchins N, Marusic I (2007) Large-scale influences in near-wall turbulence. *Philos Trans A Math Phys Eng Sci* 365:647–664.
58. Jiménez J, Hoyas S (2008) Turbulent fluctuations above the buffer layer of wall-bounded flows. *J Fluid Mech* 611:215–236.
59. Lee YH, Sung HJ (2011) Very-large-scale motions in a turbulent boundary layer. *J Fluid Mech* 673:80–120.
60. Mathis R, Hutchins N, Marusic I (2009) Large-scale amplitude modulation of the small-scale structures in turbulent boundary layers. *J Fluid Mech* 628:311–337.
61. Balint JL, Wallace JM, Vukoslavcevic P (1991) The velocity and vorticity fields of a turbulent boundary layer. Part 2. Statistical properties. *J Fluid Mech* 228:53–86.
62. Purtell LP, Klebanoff PS, Buckley FT (1981) Turbulent boundary layer at low Reynolds number. *Phys Fluids (1994)* 24:802–811.
63. Erm LP, Joubert PN (1991) Low-Reynolds-number turbulent boundary layers. *J Fluid Mech* 230:1–44.
64. Roach PE, Brierley DH (1990) The influence of a turbulent freestream on zero pressure gradient transitional boundary layer development, part I: Test cases T3A and T3B. *Numerical Simulation of Unsteady Flows and Transition to Turbulence*, eds Pironneau O, Rodi W, Ryhming IL, Savill AM, Truong TV (Cambridge Univ Press, Cambridge, UK), pp 319–347.
65. Schlatter P, Örlü R (2010) Assessment of direct numerical simulation data of turbulent boundary layers. *J Fluid Mech* 659:116–126.
66. Nagata K, Sakai Y, Komori S (2011) Effects of small-scale freestream turbulence on turbulent boundary layers with and without thermal convection. *Phys Fluids (1994)* 23:065111.
67. Hancock PE, Bradshaw P (1989) Turbulence structure of a boundary layer beneath a turbulent freestream. *J Fluid Mech* 205:45–76.
68. Sharp NS, Neuscamman S, Warhaft Z (2009) Effects of large-scale freestream turbulence on a turbulent boundary layer. *Phys Fluids (1994)* 21:095105.
69. Westin KJA, Boiko AV, Klingmann BGB, Kozlov VV, Alfredsson PH (1994) Experiments in a boundary layer subjected to freestream turbulence. I. Boundary layer structure and receptivity. *J Fluid Mech* 281:193–218.
70. Andersson P, Berggren M, Henningson DS (1999) Optimal disturbances and bypass transition in boundary layers. *Phys Fluids (1994)* 11:134–150.